A model for the conversion of ionbeam energy into thermal radiation

M. M. Basko

Citation: Physics of Fluids B: Plasma Physics (1989-1993) **4**, 3753 (1992); doi: 10.1063/1.860330
View online: http://dx.doi.org/10.1063/1.860330
View Table of Contents: http://scitation.aip.org/content/aip/journal/pofb/4/11?ver=pdfcov
Published by the AIP Publishing

A model for the conversion of ion-beam energy into thermal radiation

M. M. Basko[a)]
Max-Planck-Institut für Quantenoptik, D-8046 Garching, Germany

(Received 8 April 1992; accepted 22 July 1992)

A model is proposed for calculating the efficiency of conversion of the energy of charged-particle beams into thermal radiation. The model is based on a simplified system of radiation hydrodynamics equations and applies to optically thick converters with high conversion efficiencies $\eta_c > 0.5$. In the case of planar geometry, a self-similar solution of the model equations is obtained. This solution is used to derive a scaling law for the beam parameters required for efficient performance of planar radiative converters. A comparison of converter materials with different Z reveals that preference should be given to low-Z elements.

I. INTRODUCTION

One of the important applications of high-power beams of charged particles is generation of thermal x-rays.[1] In particular, conversion of the ion-beam energy into x-radiation is considered as a promising way to solve the problem of symmetrization and achieve a spherical implosion of deuterium–tritium capsules in thermonuclear targets driven by the beams of heavy ions.[2–4] To be of practical interest for controlled fusion, the beam-to-radiation energy conversion must be accomplished with high efficiency, $\eta_c \gtrsim 0.5$. Hence, one of the important objectives of any theoretical analysis of the converter performance should be to find minimum requirements for the ion beam parameters that ensure high values of the conversion efficiency. And it is desirable to formulate these requirements in the form of simple scaling laws that could be used for parametric analysis and optimization of the driver-target complex as a whole.

In most of the previous studies of the beam-to-radiation conversion process,[3,5–7] the authors combined radiation-hydrodynamics code simulations with a qualitative physical analysis, using the latter to derive key combinations of physical parameters that define the scaling. Arnold and Tahir[8] proposed a very simple interpolative-type formula for the conversion efficiency of cylindrical converters with a single scaling parameter. The basic physics governing the converter performance has been discussed in detail by Murakami *et al.*[6]

In this paper, we propose a model for calculating the efficiency of radiative converters driven by the beams of charged particles, which is based on a simplified system of radiation hydrodynamics equations (Sec. II). The model is adequate for optically thick converters in the limit of high values of the conversion efficiency $\eta_c > 0.5$. In the case of planar geometry, the equations of our model admit a self-similar solution, provided that the equation of state and the Rosseland mean-free path are approximated as power-law functions of temperature and density (Sec. III). In Sec. IV, we derive this solution and discuss its properties in detail. In Sec. V, the self-similar solution is applied to obtain constraints on the ion beam parameters and to compare the performance of planar converters made of materials with different Z.

II. BASIC MODEL

Fast charged particles have relatively long ranges in matter, $\Delta m \simeq 0.01$–1 g/cm^2, and deposit their energy over a substantial mass. Consequently, a characteristic feature of radiative converters irradiated by the beams of charged particles is that they are heated simultaneously over their entire (or a considerable fraction of the entire) mass. The two main physical processes that govern the performance of such converters are the hydrodynamic expansion and the transport of radiation out of the heated converter interior.

As was demonstrated by Murakami *et al.*,[6] the working cycle of an efficiently performing converter can be divided into two stages. During the first stage, the converter is heated up to its working temperature and radiates only weakly, while at the second stage the beam energy is steadily transformed into thermal radiation and escapes the converter. Accordingly, we can identify three time scales that characterize the dynamical behavior of the converter and determine its efficiency, namely, the time of heating t_h, the hydrodynamic time scale t_s, and the beam pulse duration t_b. Of course, the second stage can occur only when $t_h < t_b$. Below we assume that this condition is always fulfilled. It means that we restrict ourselves to converters with relatively long working cycles and exclude the class of "short-pulse" converters, in which the radiative stage is essentially nonsteady.

For most practical purposes, the dynamics of a radiative converter can be adequately described by the equations of one-temperature hydrodynamics with radiative heat conduction. Our basic simplifying assumption concerns the energy equation, which can be written as

$$T\frac{Ds}{Dt} = \frac{1}{\rho}\operatorname{div}\left(\frac{16}{3}\sigma_{\mathrm{SB}}\, l_{\mathrm{R}} T^3 \nabla T\right) + q_b\,, \tag{1}$$

where s is the specific entropy, $D/Dt \equiv \partial/\partial t + \mathbf{u}\cdot\nabla$ is the Lagrangian time derivative, l_{R} is the Rosseland mean-free

[a)]Permanent address: Institute of Theoretical and Experimental Physics, B. Cheremushkinskaja 25, 117259 Moscow, Russia.

 0899-8213/92/113753-11$04.00

path, σ_{SB} is the Stefan–Boltzmann constant, q_b is the rate of energy deposition per unit mass by the beam particles. During the heating stage the first term on the right-hand side of Eq. (1) is small compared to the remaining two. At this stage $q_b \approx T(Ds/Dt) \approx \epsilon_h/t_h$, where ϵ_h is a characteristic value of the specific internal energy at the end of the heating stage. In the course of the radiative stage $T|Ds/Dt| \approx \epsilon_h/t_s$, while $q_b \approx \epsilon_h/t_h$. Hence, if $t_h \ll t_s$, the left-hand side of Eq. (1) is small compared to each term on its right-hand side, and Eq. (1) can be solved under the steady-state approximation $T(Ds/Dt)=0$.

Summing up, we propose to describe the dynamics of radiative converters with the following system of equations:

$$\frac{\partial \rho}{\partial t} + \mathrm{div}(\rho \mathbf{u}) = 0, \tag{2}$$

$$\frac{\partial \mathbf{u}}{\partial t} + (\mathbf{u}\cdot\nabla)\mathbf{u} + \frac{1}{\rho}\nabla p = 0, \tag{3}$$

$$\mathrm{div}\left(\frac{16}{3}\sigma_{SB} l_R T^3 \nabla T\right) + \rho q_b = 0. \tag{4}$$

The steady-state approximation used in Eq. (4) is valid in the limit $t_h \ll t_s$. We assume that this condition is fulfilled during the entire period of illumination, $0 \leqslant t \leqslant t_b$, and that $t_h < t_b$. (Note that the relationship between t_b and t_s can be arbitrary.) Having solved Eqs. (2)–(4), we can calculate the time evolution of the total kinetic, $E_{kin}(t)$, and thermal, $E_{th}(t)$, energies of the converter. Once these energies are found, the radiative conversion efficiency can be calculated as

$$\eta_c = 1 - \frac{E_{kin}(t_b) + E_{th}(t_b)}{E_d(t_b)}. \tag{5}$$

Here, $E_d(t_b)$ is the total energy deposited in the converter over the time interval $0 \leqslant t \leqslant t_b$.

Virtually, this approach is an application of the method of successive approximations for calculating the conversion efficiency η_c when $1-\eta_c \ll 1$. Indeed, Eqs. (2)–(4) do not conserve the total energy

$$E_d(t) = E_{kin}(t) + E_{th}(t) + E_{rad}(t), \tag{6}$$

where $E_{rad}(t)$ is the radiation energy that escapes the converter by time t. If we consider the ratios $E_{kin}(t)/E_d(t)$ and $E_{th}(t)/E_d(t)$ to be small parameters, then Eq. (4) is written in the zeroth approximation, $E_{rad}(t) \approx E_d(t)$, with respect to these parameters. By solving it, we calculate the temperature distribution in the zeroth approximation. (Usually, due to a strong temperature dependence of the radiative heat conductivity, $l_R T^3 \propto T^n$ with $n \simeq 4$–7, this approximate temperature distribution is quite accurate.) Then, by combining the temperature distribution found in this way with the mass and momentum equations (2) and (3), we calculate $E_{kin}(t)$ and $E_{th}(t)$ in the first approximation. And, as a final step, we use the exact law of energy conservation (6) to evaluate the radiated energy $E_{rad}(t)$ and the conversion efficiency η_c in the first approximation with respect to E_{kin}/E_d and E_{th}/E_d.

By evaluating the energies in Eq. (5) at $t=t_b$, we neglect the radiation that emerges from the converter after the beam pulse is turned off. In the total, this tail emission may amount to a considerable fraction of $E_{th}(t_b)$. Since, however, its characteristics are highly nonsteady and the conclusion about its usefulness may depend on a particular application scheme, we simply ignore it here. One might argue also that it would be more appropriate to use $E_{kin}(t_b - t_h)$ and $E_{th}(t_b - t_h)$ instead of $E_{kin}(t_b)$ and $E_{th}(t_b)$ in Eq. (5) because a quasisteady regime described by Eq. (4) sets in only at $t=t_h$. In general, however, such a modification would not imply any dramatic improvement in the accuracy of the model, while the ultimate expressions for η_c would become more complicated.

Equations (1) and (4) are written under the assumption that the converter is in local thermodynamic equilibrium, i.e., electrons, ions, and radiation have one and the same temperature T. In relatively dense plasmas of elements with $Z \geqslant 4$, typical for radiative converters, electrons and ions come into equilibrium on a time scale much shorter than t_h, and the assumption of $T_e = T_i$ is completely justified. For radiation to be in equilibrium with matter, the Rosseland optical thickness of the converter must be $\tau_R \gg 1$. The same condition is needed to justify the diffusion approximation used in Eqs. (1) and (4). In practice, however, quite accurate results can be obtained even for $\tau_R \gtrsim 1$–2, provided that an appropriate boundary condition for Eq. (4) is used (for more details see Sec. IV A below).

III. EQUATION OF STATE AND OPACITY

With an intention to look for self-similar solutions, we adopt power-law approximations for the equation of state and the Rosseland mean-free path of the converter material:

$$p = p_* v^{-\alpha} T^{\beta}, \tag{7}$$

$$\epsilon = \frac{p_*}{\gamma_s - 1} v^{1-\alpha} T^{\beta}, \tag{8}$$

$$l_R = l_* v^{\lambda} T^{\mu}. \tag{9}$$

Here p is the pressure, ϵ the specific internal energy, l_R the Rosseland mean-free path, $v \equiv 1/\rho$ the specific volume, and

$$\gamma_s \equiv \left(\frac{\partial \ln p}{\partial \ln \rho}\right)_s = 1 + \frac{1-\alpha}{\beta - 1} \tag{10}$$

is the adiabatic index. We assume that either $\alpha < 1$ and $\beta > 1$, or $\alpha = \beta = 1$. Expressions (7) and (8) are thermodynamically consistent in the sense that they obey the basic thermodynamic identity

$$\left(\frac{\partial \epsilon}{\partial v}\right)_T = T\left(\frac{\partial p}{\partial T}\right)_v - p. \tag{11}$$

The specific values of constants p_*, l_*, α, β, λ, μ for a selection of elements throughout the periodic table, adjusted for temperature and density intervals 200 eV $< T <$ 500 eV, 0.3 g/cm^3 $< \rho <$ 3 g/cm^3, are given in Table I. The equation-of-state constants p_*, α, β, and γ_s have been calculated by using the mean-ion model from Ref. 9. Typ-

TABLE I. Equation-of-state and opacity parameters, eigenvalues, and structural constants for a selection of elements with different Z.

Parameter	D	Be	C	Al	Fe	Ag	Au
p_* ($g^{1-\alpha}$ $cm^{3\alpha-1}$ sec^{-2} $eV^{-\beta}$)	9.65×10^{11}	5.23×10^{11}	4.84×10^{11}	1.99×10^{11}	5.44×10^{10}	1.39×10^{10}	9.13×10^{9}
α	1	0.9976	0.987	0.937	0.880	0.837	0.843
β	1	1.0042	1.025	1.145	1.327	1.512	1.525
γ_s	5/3	1.57	1.52	1.43	1.37	1.32	1.30
l_* (g^{λ} $cm^{1-3\lambda}$ $eV^{-\mu}$)	2.81×10^{-8}	1.7×10^{-11}	6.3×10^{-16}	2.0×10^{-8}	9.0×10^{-9}	4.6×10^{-8}	1.0×10^{-6}
λ	2	1.80	1.85	1.30	1.30	1.22	1.24
μ	3.5	4.2	5.6	2.0	2.0	1.65	1.18
ν	1.133	1.096	1.078	0.994	0.946	0.898	0.914
Λ_1	1.675	1.660	1.648	1.660	1.660	1.666	1.685
Λ_2	1.638	1.532	1.581	1.201	1.201	1.145	1.151
Λ_E	0.886	0.901	0.913	0.901	0.901	0.895	0.877
Λ_R	1.088	1.202	1.302	1.150	1.150	1.140	1.076

ical errors of power-law formulas (7), (8) in the above-mentioned range of T, and ρ values are 10%–20%.

The values of l_*, λ, and μ in Table I have been calculated by summing the contributions of free–free, bound–free, and bound–bound transitions together with that of Compton scattering (with the exception of deuterium for which Compton scatteriung was neglected). The combined contribution of bound–bound and bound–free transitions was evaluated according to the model from Ref. 10. Deuterium is included in Table I not because it is considered to be a plausible converter material but rather as an extreme example of purely free–free absorbing medium. Note that the temperature and density dependence of l_R is in general much less regular than that of p and ϵ, and the error of Eq. (9) with constants from Table I may be very large outside the above-mentioned regions of T and ρ values.

IV. SELF-SIMILAR SOLUTIONS FOR PLANAR CONVERTERS

A. Equations in Lagrangian form and boundary conditions

Consider a plane-parallel converter symmetric with respect to the central plane $r=0$. We introduce the Lagrangian mass coordinate

$$m(t,r)=\int_0^r \rho(t,r')dr' \tag{12}$$

as independent variable and consider solutions only in the region $0\leqslant m\leqslant m_0$, where $m_0=\int_0^\infty \rho\, dr$ is the half-thickness of the converter. We assume the heating rate q_b (ergs g^{-1} sec^{-1}) to be constant in space and time within the time interval $0\leqslant t\leqslant t_b$—which is a good first approximation to the energy deposition by fast charged particles with a box-shaped temporal power profile [generalization to $q_b=q_b(t,m)$ is straightforward]. Then, Eqs. (2)–(4) take the form

$$\frac{\partial v}{\partial t}-\frac{\partial u}{\partial m}=0, \tag{13}$$

$$\frac{\partial u}{\partial t}+\frac{\partial p}{\partial m}=0, \tag{14}$$

$$\frac{16}{3}\sigma_{SB}\, l_* v^{\lambda-1}T^{\mu+3}\frac{\partial T}{\partial m}+mq_b=0. \tag{15}$$

Equation (15) is the first integral of Eq. (4) with the boundary condition $(\partial T/\partial m)_{m=0}=0$.

The boundary condition for the heat flow equation (15) deserves special attention because, as is well known,[11] a judicious choice of the boundary condition for the diffusion approximation can significantly improve its accuracy in situations when the relevant optical thickness is of order unity. In our case, this boundary condition must reflect the fact that there is no incoming radiative flux. Strictly speaking, the latter means that radiation is out of thermal equilibrium near the boundary surface. But if we assume that (1) the boundary layer is in a steady state, (2) the emission and absorption coefficients are related by the Kirchhoff–Planck law, and (3) the absorption coefficient does not depend on frequency (gray approximation), we can calculate the spectrum-integrated mean intensity J of the radiation field at the boundary surface as

$$J\overset{\text{def}}{=}\frac{1}{2}\int_0^\pi \sin\theta\, d\theta\int_0^\infty I_\nu(\theta)d\nu=\frac{\sigma_{SB}T^4}{\pi}, \tag{16}$$

where $I_\nu(\theta)$ is the specific intensity of radiation traveling in direction θ with frequency ν, θ is the angle between the direction of photon propagation and the normal to the boundary surface, T is the *matter* temperature at the boundary surface. If, in addition, we postulate the simplest angular dependence

$$I_\nu(\theta)=\begin{cases} I_{0\nu}, & 0\leqslant\theta<\pi/2,\\ 0, & \pi/2\leqslant\theta\leqslant\pi,\end{cases} \tag{17}$$

compatible with the zero incoming flux, we calculate the outgoing flux to be

$$S\overset{\text{def}}{=}2\pi\int_0^\pi \sin\theta\cos\theta\, d\theta\int_0^\infty I_\nu(\theta)d\nu=2\pi J=2\sigma_{SB}T^4. \tag{18}$$

Combined with the diffusion expression for the radiative heat flux, $S=-\frac{16}{3}\sigma_{SB}l_R T^3\nabla T$, Eq. (18) leads to the following boundary condition at $m=m_0$:

$$-\frac{16}{3}\sigma_{SB}l_*v^{\lambda-1}T^{\mu+3}\frac{\partial T}{\partial m}=2\sigma_{SB}T^4. \tag{19}$$

A reasonable estimate of the accuracy of the diffusion approximation at optical depths $\tau\sim 1$ can be obtained from the following comparison. Consider an atmosphere with a constant outward flux S in the gray approximation. The solution of the diffusion equation with the boundary condition (18) is

$$J(\tau)=\frac{3}{4\pi}S\left(\tau+\frac{2}{3}\right), \tag{20}$$

while the exact solution[12] is given by

$$J(\tau)=\frac{3}{4\pi}S[\tau+q(\tau)], \tag{21}$$

where $q(\tau)$ is a monotonic function varying between $q(0)=1/\sqrt{3}\approx 0.577$ and $q(\infty)\approx 0.71$. Thus, in case of $\tau_R\sim 1$, we expect the typical error in the quantity T^4 to be $\sim 20\%$.

The boundary condition

$$u(t,0)=0 \tag{22}$$

for the fluid velocity is a trivial consequence of symmetry with respect to $m=0$. And as the third boundary condition, we adopt not just zero pressure at $m=m_0$ but, anticipating $u(t,m_0)=\infty$, a more stringent condition of zero work done by external forces on the converter:

$$p(t,m_0)u(t,m_0)=0. \tag{23}$$

B. Dimensional analysis

If we express T in terms of p and v by virtue of Eq. (7), we find that the dependent variables v, u, and p in Eqs. (13)–(15) are determined by the following set of governing variables and parameters:

$$t,\ m,\ m_0,\ A_1\equiv\frac{\sigma_{SB}l_*}{q_b p_*^{(\mu+4)/\beta}},\quad A_2\equiv\frac{l_*}{p_*^{\mu/\beta}}. \tag{24}$$

The last parameter A_2 originates from the boundary condition (19).

None of the five parameters in Eq. (24) refers to the initial state of the converter, and in general three of them have independent dimensions. Hence, the asymptotic behavior of any solution to Eqs. (13)–(15) in the limit of strong expansion, when the dependence on the initial conditions becomes negligible, is completely determined by the values of three dimensional (say t, m_0, and A_1) and two dimensionless parameters. An obvious choice for the first dimensionless variable is

$$\xi=m/m_0. \tag{25}$$

The second dimensionless variable must be composed of t, m_0, A_1, and A_2. If, however, time can be excluded and a dimensionless combination can be formed from the constants m_0, A_1, and A_2, the asymptotic solutions of Eqs. (13)–(15) become necessarily self-similar. One readily ascertains that the latter is possible only for $\lambda=1$.

When $\lambda\neq 1$, self-similar solutions to Eqs. (13)–(15) are still possible if we replace the nonuniform boundary condition (19) with a simpler but less accurate uniform one,

$$T(t,m_0)=0. \tag{26}$$

A comparison of the two self-similar solutions, obtained, respectively, with the boundary conditions (19) and (26) for $\lambda=1$ (see Sec. IV C 2 below), shows that the uniform boundary condition (26) leads to fairly accurate values of the conversion efficiency η_c provided that $\tau_R\equiv\int_0^{m_0}l_R^{-1}v\,dm > 2$.

C. Self-similar solutions

We look for a solution of Eqs. (13)–(15) in the form

$$\begin{aligned} &r(t,m)=r_0(t)\tilde{r}(\xi),\quad u(t,m)=\dot{r}_0(t)\tilde{r}(\xi),\\ &v(t,m)=v_0(t)\tilde{v}(\xi),\quad T(t,m)=T_0(t)\tilde{T}(\xi), \end{aligned} \tag{27}$$

where ξ is defined by Eq. (25). Here and below a dot above the quantities with subscript "0" indicates differentiation with respect to time. To get rid of the extra freedom introduced by the separation ansatz (27), we fix the normalizations of $\tilde{v}$ and $\tilde{T}$

$$\tilde{v}(0)=1,\quad \tilde{T}(0)=1, \tag{28}$$

as well as the separation constant in the separation ansatz for Eq. (13),

$$\frac{m_0v_0}{r_0}=\frac{m_0\dot{v}_0}{\dot{r}_0}=\frac{1}{\tilde{v}}\frac{d\tilde{r}}{d\xi}=1. \tag{29}$$

The separation ansatz for Eqs. (14) and (15) is

$$\frac{m_0v_0^\alpha}{p_*T_0^\beta}\ddot{r}_0=-\frac{1}{\tilde{r}}\frac{d}{d\xi}\left(\frac{\tilde{T}^\beta}{\tilde{v}^\alpha}\right)=\Lambda_1, \tag{30}$$

$$\frac{3(\mu+4)}{32\sigma_{SB}}\frac{q_bm_0^2}{l_*v_0^{\lambda-1}T_0^{\mu+4}}=-\frac{\tilde{v}^{\lambda-1}}{2\xi}\frac{d\tilde{T}^{\mu+4}}{d\xi}=\Lambda_2. \tag{31}$$

To proceed further, we have to choose between the boundary conditions (19) and (26). First, we consider a more general case of arbitrary λ with boundary condition (26), and then discuss briefly a particular solution for $\lambda=1$ with boundary condition (19).

1. Arbitrary λ, boundary condition (26)

The spatial part of Eqs. (30) and (31) reduces to the following eigenvalue problem:

$$\frac{d^2\psi}{d\xi^2}+\Lambda_1(\varphi^{\beta/(\mu+4)}\psi^{-1})^{1/\alpha}=0, \tag{32}$$

$$\frac{d\varphi}{d\xi}+2\Lambda_2\xi(\varphi^{\beta/(\mu+4)}\psi^{-1})^{(1-\lambda)/\alpha}=0, \tag{33}$$

$$\psi(0)=\varphi(0)=1,\quad \frac{d\psi(0)}{d\xi}=\psi(1)\,\frac{d\psi(1)}{d\xi}=\varphi(1)=0, \tag{34}$$

where we have denoted

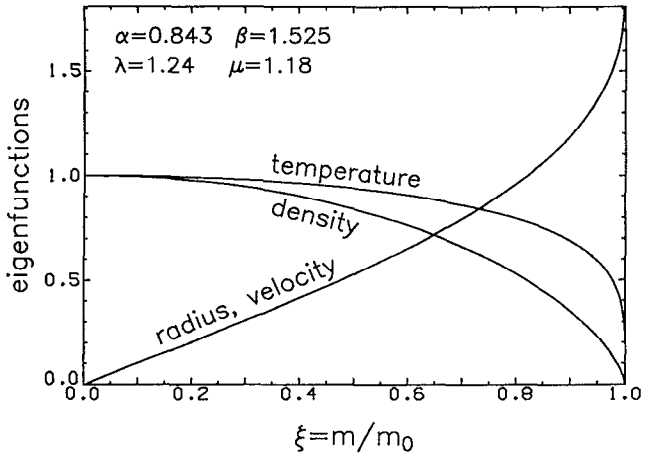

FIG. 1. Self-similar temperature, density and radius (the distance from the midplane) profiles in a planar radiative converter as calculated from Eqs. (32)–(35) for the values of parameters α, β, λ, μ corresponding to gold in Table I; m_0 [g/cm^2] is the half-thickness of the converter. The velocity profile is identical with the radius profile, see Eq. (27).

$$\psi \equiv \tilde{v}^{-\alpha}\tilde{T}^{\beta}, \quad \varphi \equiv \tilde{T}^{\mu+4}. \tag{35}$$

Table I lists the eigenvalues Λ_1 and Λ_2 as calculated from Eqs. (32)–(34) for seven different elements. Figure 1 displays the eigenfunctions $\tilde{r}(\xi)$, $\tilde{p}(\xi) \equiv \tilde{v}^{-1}(\xi)$ and $\tilde{T}(\xi)$ for the values of α, β, λ, μ corresponding to gold in Table I.

It should be noted here that a solution to Eqs. (32) and (33) with the boundary conditions (34) exists not for any combination of parameters α, β, λ, μ. When we examine the behavior of $\psi(\xi)$ and $\varphi(\xi)$ in the limit $\xi \to 1$, we find that the boundary condition (23) implies a restriction

$$\alpha > \frac{1}{3} - \frac{\beta}{\mu+4}\left(\lambda - \frac{1}{3}\right). \tag{36}$$

In practice (see Table I), inequality (36) holds with a wide margin. It can be proved also that for

$$\frac{1}{3} - \frac{\beta}{\mu+4}\left(\lambda - \frac{1}{3}\right) < \alpha < 1 - \frac{\beta\lambda}{\mu+4} \tag{37}$$

$\lim_{\xi \to 1} \tilde{r}(\xi) = \infty$ and the converter extends to infinity, while for

$$\alpha > 1 - \frac{\beta\lambda}{\mu+4}, \tag{38}$$

it is finite [$\tilde{r}(1) < \infty$]. All parameter combinations from Table I lead to finite values of $r(t, m_0) = r_0(t)\tilde{r}(1)$.

Having introduced the expansion factor

$$X(t) \equiv \frac{v_0(t)}{v_{00}}, \tag{39}$$

with v_{00} being the initial specific volume in the converter center, we can transform the temporal part of the separation ansatz (30) and (31) to

$$T_0(t) = T_{00} X^{(1-\lambda)/(\mu+4)}, \tag{40}$$

$$v_0^2 \equiv v_{00}^2 \dot{X}^2 = 2\Lambda_1 p_* m_0^{-2} v_{00}^{1-\alpha} T_{00}^{\beta} \begin{cases} \dfrac{X^{1-\nu}-1}{1-\nu}, & \nu \neq 1, \\ \ln X, & \nu = 1, \end{cases} \tag{41}$$

where

$$\nu = \alpha + \frac{\beta(\lambda-1)}{\mu+4}. \tag{42}$$

The initial temperature T_{00} in the converter center is given by

$$T_{00} = \left(\frac{3(\mu+4)}{32\Lambda_2}\frac{q_b m_0^2}{\sigma_{SB} l_*} v_{00}^{1-\lambda}\right)^{1/(\mu+4)}. \tag{43}$$

The solution of Eq. (41) for $X(t)$ can be written in an implicit form as

$$\frac{t}{t_s} = \begin{cases} (2\Lambda_1)^{-1/2} \displaystyle\int_1^X \left(\frac{1-\nu}{\xi^{1-\nu}-1}\right)^{1/2} d\xi, & \nu \neq 1, \\ \left(\dfrac{2}{\Lambda_1}\right)^{1/2} \displaystyle\int_1^{\sqrt{\ln X}} \exp(\xi^2) d\xi, & \nu = 1, \end{cases} \tag{44}$$

where

$$t_s = \frac{m_0 v_{00}}{(p_* v_{00}^{1-\alpha} T_{00}^{\beta})^{1/2}} \tag{45}$$

is, apart from the insignificant numerical factor $\alpha^{-1/2}$, the time of isothermal sound propagation across the initial converter half-thickness $m_0 v_{00}$.

For $\nu < 1$ (typical for high-Z materials), Eq. (41) admits an important asymptotic solution

$$v_0(t) = \left[\frac{\Lambda_1(1+\nu)^2}{2(1-\nu)} p_* m_0^{-2} \times \left(\frac{3(\mu+4)}{32\Lambda_2}\frac{q_b m_0^2}{\sigma_{SB} l_*}\right)^{\beta/(\mu+4)} t^2\right]^{1/(1+\nu)}, \tag{46}$$

valid in the limit $v_0^{1-\nu} \gg v_{00}^{1-\nu}$. This solution does not depend on the initial specific volume v_{00} (starts from $v_{00}=0$). Its physical meaning is as follows: In the limit of a very strong expansion, when $t \gg t_s$ implies $[X(t)]^{1-\nu} \gg 1$, the converter dynamics is governed by Eq. (46) [together with Eqs. (32), (33), (40), and (43)] *independent of the initial conditions*. In contrast, the "general" solution (44), starting from nonzero v_{00}, is valid only when the initial density distribution conforms to the eigenfunctions determined by Eqs. (32)–(34). In reality, however, expanding converters approach the asymptotic solution (46) rather slowly. As can be seen from Table I, even for the heaviest elements $1-\nu \lesssim 0.1$; hence, unrealistically high values of the expansion factor, $X \gtrsim 10^{10}$, are needed to reach, say, $X^{1-\nu} \gtrsim 10$.

The thermal and kinetic energies of the converter are given by

$$E_{th}(t) = m_0 \int_0^1 \epsilon \, d\xi = \frac{\Lambda_E}{\gamma_s - 1} m_0 p_* v_{00}^{1-\alpha} T_{00}^{\beta} X^{1-\nu}, \tag{47}$$

$$E_{\rm kin}(t)=m_0\int_0^1\frac{u^2}{2}\,d\xi$$

$$=\Lambda_E m_0 p_* v_{00}^{1-\alpha}T_{00}^{\beta}\begin{cases}\dfrac{X^{1-\nu}-1}{1-\nu}, & \nu\neq 1,\\ \ln X, & \nu=1,\end{cases}\qquad(48)$$

where

$$\Lambda_E=\int_0^1\tilde{v}^{1-\alpha}\tilde{T}^{\beta}\,d\xi$$

$$=\int_0^1\psi\tilde{v}\,d\xi$$

$$=\int_0^1\psi^{1-1/\alpha}\varphi^{\beta/\alpha(\mu+4)}\,d\xi.\qquad(49)$$

Numerical values of Λ_E are listed in Table I. In deriving Eq. (48), we have invoked the identity

$$\Lambda_1\int_0^1\tilde{r}^2\,d\xi=\Lambda_E,\qquad(50)$$

which can be easily verified by virtue of Eqs. (30), (32)–(34). Finally, substituting Eqs. (47) and (48) into Eq. (5), we obtain the conversion efficiency,

$$\eta_c=1-\Lambda_E\frac{t_h}{t_b}\Gamma_b,\qquad(51)$$

where

$$t_h\equiv\frac{\epsilon_{00}}{q_b}=\frac{p_* v_{00}^{1-\alpha}T_{00}^{\beta}}{(\gamma_s-1)q_b}\qquad(52)$$

is the time needed to heat the converter center up to the working temperature T_{00}, $\Gamma_b\equiv\Gamma(t_b/t_s)$ is the ratio of the total nonradiative energy losses to the energy spent on the heating of the converter, and

$$\Gamma\left(\frac{t}{t_s}\right)=\begin{cases}X^{1-\nu}+\dfrac{\gamma_s-1}{1-\nu}\,(X^{1-\nu}-1), & \nu\neq 1,\\ 1+(\gamma_s-1)\ln X, & \nu=1,\end{cases}\qquad(53)$$

with $X(t/t_s)$ determined by Eq. (44).

We do not present here lengthy expressions for $E_{\rm th}(t)$, $E_{\rm kin}(t)$, and η_c in the asymptotic case of $X^{1-\nu}\gg 1$ (for $\nu<1$), when these quantities cease to depend on the initial conditions. We note only that in this limit the ratio between the kinetic and internal energies approaches a constant (time independent) value

$$\frac{E_{\rm kin}(t)}{E_{\rm th}(t)}=\frac{\gamma_s-1}{1-\nu},\qquad(54)$$

determined by individual properties of the converter material.

From Eq. (51), it is seen that we can distinguish two limiting cases of the converter performance. In the near-static limit $t_b\ll t_s$, when $\Gamma_b-1\ll 1$, the nonradiative energy losses are due only to the initial converter heating and Eq. (51) gives a conceptually very transparent (apart from the structural constant Λ_E) answer for η_c. Note that in this limit the conversion efficiency can be easily calculated for any initial density distribution by solving Eq. (15) alone and ignoring the contribution of $E_{\rm kin}$. In the opposite limit of strong expansion, when $\Gamma_b\gg 1$, the kinetic energy dominates in the total nonradiative energy losses; in the case of high-Z converters its relative contribution approaches a time-independent limit given by Eq. (54).

TABLE II. Eigenvalues and structural constants for $\lambda=1$.

	$\alpha=1.0$, $\beta=1.0$, $\mu=3.5$;			$\alpha=0.8$, $\beta=1.6$, $\mu=1.0$;		
δ	Λ_1	Λ_E	Λ_R	Λ_1	Λ_E	Λ_R
0	1.635	0.927	1.502	1.660	0.902	1.150
0.1	1.624	0.941	1.298	1.631	0.941	1.107
1.0	1.595	0.974	1.103	1.546	1.049	1.042
10	1.575	0.996	1.015	1.487	1.127	1.006

The Rosseland optical thickness (actually half-thickness) of the converter is given by

$$\tau_{\rm R}(t)\equiv m_0\int_0^1 l_{\rm R}^{-1}v\,d\xi=\Lambda_{\rm R}\frac{m_0 v_{00}^{1-\lambda}}{l_* T_{00}^{\mu}}X^{4(1-\lambda)/(\mu+4)},\qquad(55)$$

where

$$\Lambda_{\rm R}=\int_0^1\psi^{(\lambda-1)/\alpha}\varphi^{-[\beta(\lambda-1)+\mu\alpha]/\alpha(\mu+4)}\,d\xi\qquad(56)$$

(numerical values of $\Lambda_{\rm R}$ are given in Table I). Typically $\lambda>1$ and $\tau_{\rm R}(t)$ decreases with time. Hence, for assessing the applicability of our model we must use $\tau_{\rm R}(t_b)$.

2. $\lambda=1$, boundary condition (19)

In this case the eigenvalue problem reduces to

$$\frac{d^2\psi}{d\xi^2}+\Lambda_1\tilde{T}^{\beta/\alpha}\psi^{-1/\alpha}=0,\qquad(57)$$

$$\psi(0)=1,\quad\frac{d\psi(0)}{d\xi}=\psi(1)\frac{d\psi(1)}{d\xi}=0,\qquad(58)$$

where

$$\varphi(\xi)\equiv\tilde{T}^{\mu+4}(\xi)=1-\frac{\xi^2}{1+\delta},\qquad(59)$$

$$\delta=\frac{16}{3(\mu+4)}\frac{l_*}{m_0}\left(\frac{q_b m_0}{2\sigma_{\rm SB}}\right)^{\mu/4}.\qquad(60)$$

The temperature distribution does not depend on time and

$$T_0\equiv T_{00}=\left(\frac{3(\mu+4)}{32}\frac{q_b m_0^2}{\sigma_{\rm SB}l_*}(1+\delta)\right)^{1/(\mu+4)}.\qquad(61)$$

All the other formulas—from Eq. (44) to Eq. (56)—obtained in the previous section remain essentially unchanged. The only exception is Eq. (46) in which Λ_2 must be replaced by $(1+\delta)^{-1}$. And one should keep in mind that $\nu\equiv\alpha$ for $\lambda=1$, while φ is given by Eq. (59). The dependence of constants Λ_1, Λ_E, $\Lambda_{\rm R}$ on δ is illustrated in Table II.

If we set $\delta=0$ in Eqs. (59) and (61), we recover the solution from Sec. IV C 1, obtained with the uniform

boundary condition (26), in the particular case of $\lambda=1$. We can use this fact to evaluate the accuracy of the uniform boundary condition (26). From Eqs. (61) and (51), we see that, by replacing a more accurate boundary condition (19) with a cruder one (26), we introduce a relative error of $\delta/(\mu+4)\simeq(0.1\text{–}0.2)\delta$ in the central temperature T_{00}, and $\delta\beta/(\mu+4)\simeq(0.1\text{–}0.3)\delta$ in the quantity $(1-\eta_c)$ (for the moment, we neglect the variation of Λ_E and Γ_b with δ). On the other hand, parameter δ is directly related to the Rosseland optical thickness of the converter,

$$\tau_R=\frac{16}{3(\mu+4)}\Lambda_R\delta^{-4/(\mu+4)}(1+\delta)^{-\mu/(\mu+4)}, \tag{62}$$

which does not depend on time for $\lambda=1$. Using the latter relationship and allowing for the δ dependence of Λ_E and Λ_R (see Table II), we find that in converters with $\tau_R\geqslant 2$ the relative error in the values of $(1-\eta_c)$ caused by using the uniform boundary condition (26) instead of (19) is $\leqslant 5\%$ for low-Z materials, and $\leqslant 15\%$ for heavy elements. Thus, we can adopt $\tau_R=2$ as a lower bound for applicability of the self-similar solution described in Sec. IV C 1.

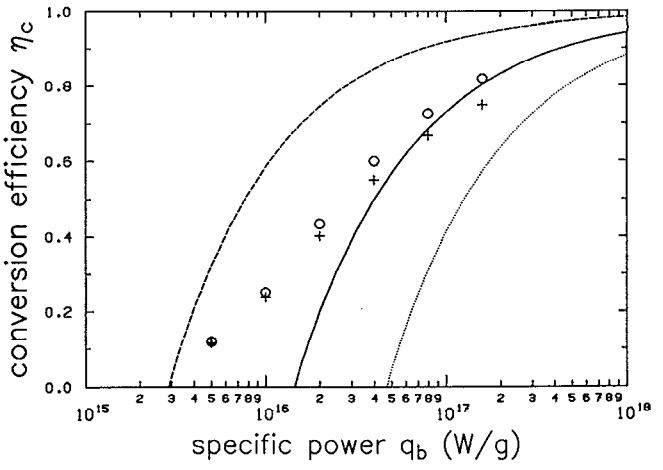

FIG. 2. Conversion efficiency η_c as a function of the specific energy deposition rate q_b for a planar gold converter with the initial half-thickness $m_0=0.1$ g/cm^2 and the initial density $\rho_{00}=20$ g/cm^3. Solid curve: full self-similar solution (51) with Γ_b given by Eq. (53); dashed curve: static limit of $\Gamma_b=1$ in Eq. (51); dotted curve: asymptotic solution (46) in the limit of strong expansion. The pulse duration $t_b=10^{-8}$ sec. The results of 1-D hydrodynamics code simulations are shown with plus signs (radiation pressure accounted for) and open circles (radiation pressure ignored).

V. SCALING LAWS AND APPLICATIONS

For a fixed converter material, the conversion efficiency η_c, as given by Eq. (51), is a function of four free parameters: q_b, t_b, m_0, and $v_{00}\equiv 1/\rho_{00}$. The first three of them are essentially the beam parameters, provided that the range of beam particles is equal to the converter thickness $2m_0$. For applications, it is important to know (1) how do the beam parameters scale with one another when the conversion efficiency is fixed at some threshold value (say, $\eta_c=0.5$) which separates efficient converters from inefficient ones, and (2) what material gives the highest conversion efficiency for a fixed combination of the beam parameters. But before addressing these issues, we examine how our approximate model and the self-similar solution compare with one-dimensional (1-D) hydrodynamics simulations.

A. Comparison with 1-D code simulations

Most critical is to test the approximations of Sec. II against strongly expanding converters, in which $X_b\gg 1$, $E_{\rm kin}(t_b)>E_{\rm th}(t_b)$, and the discrepancy between our model and the exact solutions of the hydrodynamics equations is expected to be the largest. Figure 2 shows the conversion efficiency η_c versus heating rate q_b as calculated for a gold converter with $m_0=0.1$ g/cm^2, $\rho_{00}=20$ g/cm^3 according to the full solution (51)–(53) (solid line) and in two opposite limits—the static limit [$\Gamma_b=1$ in Eq. (51), dashed line] and the asymtotic limit of strong expansion [Eq. (46), dotted line]. The beam pulse duration t_b is fixed at 10^{-8} sec. In this example the working temperature in the converter center, the heating and sonic time scales vary with the relevant free parameters as

$$T_{00}[\text{eV}]=760\left(\frac{q_b}{10^{16}\ \text{W/g}}\right)^{0.193}\left(\frac{m_0}{0.1\ \text{g/cm}^2}\right)^{0.386}\times\left(\frac{\rho_{00}}{20\ \text{g/cm}^3}\right)^{0.0463}, \tag{63}$$

$$t_h[\text{sec}]=4.7\times 10^{-9}\left(\frac{q_b}{10^{16}\ \text{W/g}}\right)^{-0.706}\left(\frac{m_0}{0.1\ \text{g/cm}^2}\right)^{0.589}\times\left(\frac{\rho_{00}}{20\ \text{g/cm}^3}\right)^{-0.0863}, \tag{64}$$

$$t_s[\text{sec}]=4.2\times 10^{-10}\left(\frac{q_b}{10^{16}\ \text{W/g}}\right)^{-0.147}\left(\frac{m_0}{0.1\ \text{g/cm}^2}\right)^{0.706}\times\left(\frac{\rho_{00}}{20\ \text{g/cm}^3}\right)^{-0.957}. \tag{65}$$

The Rosseland optical thickness, given by

$$\tau_R(t)=88\left(\frac{q_b}{10^{16}\ \text{W/g}}\right)^{-0.228}\left(\frac{m_0}{0.1\ \text{g/cm}^2}\right)^{0.544}\times\left(\frac{\rho_{00}}{20\ \text{g/cm}^3}\right)^{0.185}[X(t)]^{-0.185}, \tag{66}$$

is always greater than unity.

A characteristic feature of every $\eta_c(q_b)$ curve calculated with our model is that it starts from $\eta_c=0$ at a certain threshold value of q_b. Below this threshold Eq. (5) yields negative values of η_c—which is a direct consequence of the method of successive approximations employed in Sec. II. The negative values of η_c should be interpreted as an indication that the true values of the conversion efficiency are rather low ($\eta_c\lesssim 0.2\text{–}0.3$) in the corresponding parameter region.

In the example illustrated by Fig. 2, the hydrodynamic energy losses are about twice as high as the energy spent on heating the converter up to the working temperature, and the "dynamic" conversion efficiency (solid curve) lies considerably below the static limit (dashed curve). On the other hand, even though the expansion factor $X(t_b)$ ranges from 90 to 190 as q_b rises from 1.5×10^{16} W/g to 10^{18} W/g, yet it is not high enough for the converter to be adequately described by the asymptotic solution (46) (dotted curve). Under such conditions, one would expect a disagreement between the self-similar solution and the hydrodynamics code simulations to be the most pronounced.

The results of 1-D code simulations shown in Fig. 2 have been obtained for a gold slab with a constant initial density profile, $\rho(0,m)=\rho_{00}=20$ g/cm^3, in two cases: with radiation pressure accounted for (plus signs) and ignored (open circles); for the equation of state and the Rosseland mean-free path the power-law approximations (7)–(9) have been used. Comparing the 1-D code results with the solid curve in Fig. 2, we conclude that (1) the approximate model of Sec. II is quite adequate for optically thick converters with high conversion efficiencies, $\eta_c\gtrsim0.5$, and (2) the self-similar solution of Sec. IV C 1 can be successfully applied to strongly expanding converters with nonself-similar initial density profiles long before the asymptotic regime (46) sets in.

From Eqs. (64) and (65) we find that $t_h>t_s$ along the solid line in Fig. 2 and the basic condition for applicability of Eq. (4), $t_h\ll t_s$, is not fulfilled. However, if we evaluate t_s for the final rather than for the initial density profile, we still find $t_h\ll t_s$—which suffices for Eq. (51) to give accurate enough values of η_c when $\eta_c>0.5$.

B. Scaling for the beam parameters

If we demand that the conversion efficiency of a planar converter $\eta_c\geqslant0.5$, we find from Eq. (51) that the beam parameters must satisfy the condition

$$q_b^{1-\beta/(\mu+4)}m_0^{-2\beta/(\mu+4)}t_b\geqslant g_*\Gamma_b\rho_{00}^{\nu-1}, \tag{67}$$

where

$$g_*=\frac{2\Lambda_E}{\gamma_s-1}p_*\left(\frac{3(\mu+4)}{32\Lambda_2\sigma_{SB}I_*}\right)^{\beta/(\mu+4)} \tag{68}$$

is a constant of material. If we assume that the beam energy is used "economically" and the converter thickness $2m_0$ coincides with the range of fast particles, inequality (67) can be readily converted into a power-law relationship between the beam intensity $I_b=2m_0q_b$ [W/cm^2], the particle energy E_b, and the pulse duration t_b—provided that the particle species is fixed and the range-energy relation is known.

For material parameters of practical interest it usually turns out that $|\nu-1|\lesssim0.1$ (see Table I). Consequently, the right-hand side of Eq. (67) depends only very weakly on ρ_{00}, q_b, m_0, and t_b (Γ_b varies between 1 in the static limit and 3–4 in strongly expanding converters). As a result, the left-hand side of Eq. (67) can be viewed as a single scaling variable whose value should exceed a certain threshold in order to ensure high efficiency of the beam-to-radiation energy conversion. In other words, Eq. (67) establishes a scaling law for the three relevant beam parameters q_b, m_0, t_b in the case of planar converter geometry. Figure 3 illustrates this scaling law on the (q_b,m_0) parametric plane for four different elements ($\eta_c=0.5$ curves).

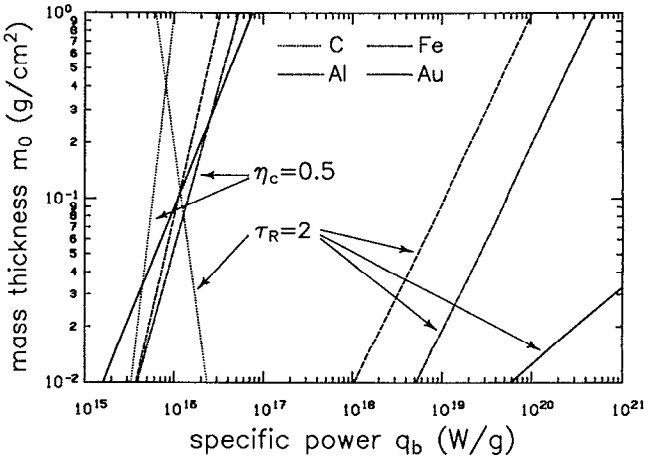

FIG. 3. For each of the four selected elements two curves are shown on the (q_b,m_0) parameter plane: the $\eta_c=0.5$ curve and the $\tau_R=2$ curve. Both families of curves have been calculated in the static limit, with $\Gamma_b=1$ in Eq. (51) and $X=1$ in Eq. (55), for $\rho_{00}=1$ g/cm^3 and $t_b=10^{-8}$ sec. As discussed in Sec. IV C 2, the self-similar solution for arbitrary λ obtained with the uniform boundary condition (26) is applicable on the left from the $\tau_R=2$ curves, where $\tau_R>2$. On the other hand, the initial equations of the model (2)–(5) are adequate on the right from the $\eta_c=0.5$ curves, where $\eta_c>0,5$. The resulting region of applicability between the $\eta_c=0.5$ and the $\tau_R=2$ curves is rather narrow for carbon (and lighter elements), and quite wide for aluminum and heavier elements. The curves $\eta_c=0.5$ illustrate also the scaling law (67).

Earlier Meyer-ter-Vehn and Unterseer[5] and Arnold and Tahir[8] proposed to use a different scaling parameter which in our notation takes the form $x=q_bm_0\rho_{00}^{-2}$. This parameter emerges from a comparison between the heating time scale t_h and the sonic time t_s, while our scaling variable on the left-hand side of Eq. (67) relates the heating time scale t_h to the pulse duration t_b. We argue that, at least for the planar converters, our result is more adequate because a strong expansion of a planar layer typically does not imply significant degradation of its optical depth and conversion efficiency. Therefore, planar converters may perform efficiently even when $t_s\ll t_h<t_b$ [here t_s is the *initial* sonic time defined by Eq. (45)] and the criterion $t_h\lesssim t_s$ used in Refs. 5 and 8 is violated.

Another conclusion that can be infered from Eq. (67) concerns the optimum value of the initial converter density ρ_{00}. If, in addition to the converter material, the beam parameters q_b, m_0, and t_b are also fixed, we are left with a single free parameter ρ_{00}. A close scrutiny of Eqs. (44), (45), and (53) reveals that the product $\Gamma_b\rho_{00}^{\nu-1}$ is a monotonically increasing function of ρ_{00} for $\nu\geqslant1$, and has a shallow minimum at a certain ρ_{00} [which corresponds to $t_s\simeq(2-3)t_b$] for $\nu<1$. Thus, in low-Z converters (for which $\nu>1$) it is advantageous to have as low as possible value of the initial density ρ_{00} (so far as the converter

remains optically thick), while in high-Z materials (for which $\nu < 1$) there is an optimum value of ρ_{00}, below which the conversion efficiency decreases with decreasing ρ_{00}.

C. Low-Z converters versus high-Z converters

Some idea on how the conversion efficiency depends on the atomic number Z of the converter material can already be infered from Fig. 3. Comparing relative positions of $\eta_c = 0.5$ curves for different elements we conclude that in thin converter foils, when $m_0 \lesssim 0.03$–0.1 g/cm^2, higher conversion efficiencies can be obtained with high-Z materials (gold), while in thicker foils, with $m_0 \gtrsim 0.1$ g/cm^2, low-Z elements are preferable. Such nontrivial behavior results from an interplay of two factors: on the one hand, high-Z elements require less energy per gram to be heated to the same temperature; on the other hand, due to higher opacity, high-Z converters must be heated to higher central temperatures than low-Z converters with the same initial thickness and density.

For a more detailed comparison, we must take into account that the converter thickness $2m_0$ is related to the range of beam particles, which is also a function of Z. Here, we choose the following approach. We assume the energy E_b of individual beam ions to be an independent variable. For each value of E_b, we calculate (1) the converter thickness $2m_0$ by using the range-energy relation for a uniform medium with temperature T_{00} and density ρ_{00}, and (2) the beam intensity $I_b = 2m_0 q_b$ from the condition that conversion efficiency η_c, as given by Eq. (51), is equal to 0.5. The results of such calculations for a beam of ^{209}Bi ions stopped in three different converter materials are shown in Fig. 4. As the range-energy relation, we used a power-law fit,

$$R(E_b,T,\rho) = R_0 \left(\frac{E_b}{10\ \text{GeV}}\right)^{1.4} \left(\frac{T}{300\ \text{eV}}\right)^{\mu_b} \left(\frac{\rho}{1\ \text{g/cm}^3}\right)^{0.13}, \tag{69}$$

to the ranges calculated from a detailed stopping-power model[13] for 3 GeV $< E_b <$ 20 GeV, 100 eV $< T <$ 1 keV, 0.1 g/cm^3 $< \rho <$ 10 g/cm^3. The values of the fit parameters R_0 and μ_b are given in Table III. For each target element two values of the initial density, namely $\rho_{00} = \rho_s \equiv$ normal solid-state density and $\rho_{00} = 0.3$ g/cm^3, have been probed. The pulse duration t_b was fixed at 10^{-8} sec.

Each curve in Fig. 4 represents a lower bound to the beam intensity I_b that is needed for the efficient beam-to-radiation energy conversion. For one and the same element, the lower initial density, $\rho_{00} = 0.3$ g/cm$^3 < \rho_s$, always corresponds to a lower beam intensity threshold. This is caused primarily by the corresponding increase of the hydrodynamic time scale t_s, almost in proportion with the decrease in ρ_{00} [see Eq. (45)]. When the pulse duration t_b is fixed, a larger value of t_s implies lower energy losses to the hydrodynamic expansion of the converter [a lower value of factor Γ_b in Eq. (51)] and, as a consequence, a lower intensity threshold for the 50% conversion efficiency. Besides, at smaller target densities fast ions have somewhat lower ranges due to a higher plasma ionization

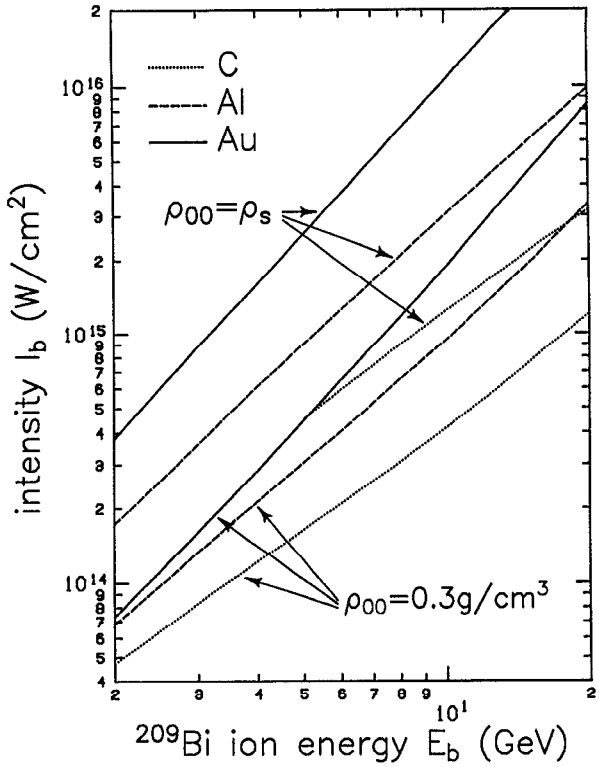

FIG. 4. Threshold beam intensity for 50% conversion efficiency as a function of ^{209}Bi ion energy. For each of the three selected elements two curves are plotted: the upper curve corresponds to the initial converter density equal to the normal solid-state density of the respective element; the lower curve corresponds to the initial density $\rho_{00} = 0.3$ g/cm^3. The difference between the upper and the lower curves for each element reflects the role of the hydrodynamic energy losses in expanding planar converters.

[cf. Eq. (69)], which also contributes to the lowering of the beam intensity threshold.

Comparing the curves for different elements in Fig. 4, we clearly see that low-Z materials are superior to heavy elements (Recently, a similar result has been obtained also by Atzeni[14].) It should be emphasized here that this conclusion is reached under the condition that the values of the initial density, used for converter materials with different Z, do not decrease with Z. Low-Z elements perform better because they have higher stopping powers per unit mass and lower Rosseland opacities. Both factors cause the Rosseland optical thickness τ_R to decrease with decreasing Z. When τ_R becomes comparable to unity, our model is no longer applicable. For this reason no results for Be are given in Figs. 3 and 4: In the parameter region considered, there exists no solution with $\eta_c > 0.5$ and $\tau_R > 1$ for the Be

TABLE III. Fit parameters for power-law approximation (69) to the ranges of ^{209}Bi ions.

Parameter	Be	C	Al	Fe	Ag	Au
R_0 (g/cm^2)	0.11	0.096	0.11	0.13	0.16	0.22
μ_b	0	0	0	−0.13	−0.20	−0.25

converters. Also, the dotted curve for carbon with $\rho_{00}=\rho_s$ is truncated at $E_b \approx 5$ GeV because $\tau_R < 1$ for smaller E_b. In carbon converters with $\rho_{00}=0.3$ g/cm^3, we find $\tau_R = 1.5$–2.2, while along both aluminum curves $\tau_R = 5$–15. Thus a recommendation for picking up the best converter material would be to take an element with the lowest possible Z for which the converter is still optically thick (optically thin converters, with $\tau_R \ll 1$, are relatively inefficient[6]).

VI. CONCLUSION

Fast charged particles, used to create high energy densities in matter, typically deposit their energy over a considerable volume of the target material, which is optically thick with respect to thermal radiation. Therefore, an adequate theoretical model for converison of the energy of intense particle beams into thermal x-rays must be based on the equations of nonsteady hydrodynamics and account for the energy transport by radiation. In optically thick converters radiation transport can be approximated as a radiative heat conduction. In this paper, we have demonstrated that, so long as one is interested in radiative converters with high conversion efficiencies, the system of hydrodynamic equations with radiative heat conduction can be simplified one step further: while retaining nonsteady terms in the mass and momentum equations, one can discard the nonsteady entropy term in the energy equation and, thereby, reduce it to a steady-state equation of radiative heat diffusion. In the particular case of planar geometry the system of thus simplified equations admits a self-similar solution, provided that power-law formulas are used for the equation of state and the Rosseland mean-free path as a function of temperature and density.

Having employed the self-similar solution to describe the performance of planar converters, we obtain an analytical expression for the beam-to-radiation conversion efficiency. Analytical formulas make it possible to carry out a complete parametric analysis of the properties of planar converters. In particular, we establish a scaling relationship (67) for the beam parameters that must be fulfilled to ensure high efficiency of the energy conversion. The physical condition $t_h \leqslant 0.5\ \Gamma_b^{-1} t_b$ that underlies this scaling implies that the heating time t_h should be small compared to the pulse duration t_b; a slowly varying factor $\Gamma_b \geqslant 1$ represents the role of the hydrodynamic expansion ($\Gamma_b = 1$ in static converters, and $\Gamma_b \simeq 3$–4 in strongly expanding converters). A comparison between low-Z and high-Z converter materials reveals that, in the parameter region typical for the inertial-confinement-fusion applications and for the same values of the initial density, low-Z converters perform more efficiently than the high-Z ones.

The model proposed here and the results obtained do not apply universally. In each particular case of practical interest the applicability of the model should be analyzed separately. In general, Eqs. (2)–(5) can be used for more complex than just planar converter geometries, provided that (1) the converter is optically thick, $\tau_R \gtrsim 1$, and (2) the conversion efficiency is high enough, $\eta_c \gtrsim 0.5$. The results presented in Sec. V indicate that there remains a wide domain in the parameter space where both conditions (1) and (2) are satisfied (at least for medium- and high-Z elements) and which might be of interest for applications. There may exist also converter configurations with intermediate optical thicknesses of, say, $\tau_R \simeq 0.1$–1 that perform quite efficiently but are beyond the applicability limits of the present model (converters with $\tau_R \ll 1$ will be inefficient because they must be heated to higher temperatures to achieve the same emissivity as those with $\tau_R \sim 1$). Clearly, such cases must be explored numerically.

The analytical results obtained in this paper for the planar converters can only be used under the additional limitation that the beam focal spot is larger than—or at least comparable to—the expansion height scale of the converter, when two- and three-dimensional effects of the plasma expansion are insignificant. Fortunately, this appears to be a rather typical case for high-current ion beams, as exemplified by the PBFA-II experiments[1] in which the focal spot radius is $\simeq 3$–5 mm.

When applied to more complex converter configurations, Eqs. (2)–(5) will, in general, admit no self-similar solutions. Nevertheless, in many cases Eq. (4) can be solved analytically, provided that a certain simple density profile is assumed. The latter means that, if one approximates the density distribution in the expanding converter by a one-parameter family of physically reasonable simple curves, it may still be possible to solve Eqs. (3) and (4) analytically and obtain approximate analytical expressions for $E_{th}(t)$, $E_{kin}(t)$, and η_c. Such approximate solutions may be very helpful in evaluating the conversion efficiency and deriving scaling laws for various types of radiative converters.

ACKNOWLEDGMENT

I appreciate stimulating discussions with S. Atzeni and J. Meyer-ter-Vehn. I am grateful to J. Meyer-ter-Vehn and S. Witkowski for providing an opportunity to stay at the Max-Planck-Institut für Quantenoptik.

This work has been supported by the German Bundesministerium für Forschung and Technologie.

[1] D. L. Cook, J. E. Bailey, K. W. Bieg, D. D. Bloomquist, R. S. Coats, G. C. Chandler, M. E. Cuneo, M. S. Derzon, M. P. Dasjarlais, P. L. Dreike, R. J. Dukart, R. A. Gerber, D. J. Johnson, R. J. Leeper, T. R. Lockner, D. H. McDaniel, J. E. Maenchen, M. K. Matzen, T. A. Mehlhorn, L. P. Mix, A. R. Moats, W. E. Nelson, T. D. Pointon, A. L. Pregenzer, J. P. Quintenz, T. J. Renk, S. E. Rosenthal, C. L. Ruiz, S. A. Slutz, R. W. Stinnett, W. A. Stygar, G. C. Tisone, J. R. Woodworth, and J. P. VanDevender, in *Proceedings of the Eighth International Conference on High-Power Particle Beams (BEAMS' 90)*, Novosibirsk, USSR, 1990; edited by B. N. Breizman and B. A. Knyazev (World Scientific, Singapore, 1991), Vol. 1, p. 3.

[2] J. H. Nuckolls, Phys. Today **35**, 24 (1982).

[3] J. D. Lindl, R. O. Bangerter, J. W-K. Mark, and Yu-Li Pan, in *Heavy Ion Inertial Fusion*, edited by M. Reiser, T. Godlove, and R. Bangerter, AIP Conference Proceedings 152 (American Institute of Physics, New York, 1986), p. 89.

[4] M. Murakami and J. Meyer-ter-Vehn, Nucl. Fusion **31**, 1315 (1991).

[5]J. Meyer-ter-Vehn and K. Unterseer, Laser Part. Beams **3**, 283 (1985).
[6]M. Murakami, J. Meyer-ter-Vehn, and R. Ramis, J. X-ray Sci. Tech. **2**, 127 (1990).
[7]S. Atzeni, Part. Accel. **37-38**, 345 (1992).
[8]R. C. Arnold and N. A. Tahir, Phys. Lett. A **137**, 281 (1989).
[9]M. M. Basko, Teplofiz. Vys. Temper. **23**, 483 (1985) [High Temper. (USSR) **23**, 388 (1985)].
[10]V. S. Imshennik, I. N. Mikhailov, M. M. Basko, and S. V. Molodtsov, Zh. Eksp. Teor. Fiz. **90**, 1669 (1986) [Sov. Phys. JETP **63**, 980 (1986)].
[11]D. Mihalas and B. Weibel Mihalas, *Foundations of Radiation Hydrodynamics* (Oxford U.P., New York, 1984), pp. 555–557.
[12]S. Chandrasekhar, *Radiative Transfer* (Dover, New York, 1960), Sec. 25.
[13]M. M. Basko, Fiz. Plazmy **10**, 1195 (1984) [Sov. J. Plasma Phys. **10**, 689 (1984)].
[14]S. Atzeni, "Scaling laws for thermal radiation generation from heavy-ion beam heated converters," to appear in Nucl. Fusion (1992).